

Design of Multistimuli Responsive Hydrogels Using Integrated Modeling and Genetically Engineered Silk–Elastin-Like Proteins

Wenwen Huang, Anna Tarakanova, Nina Dinjaski, Qin Wang, Xiaoxia Xia, Ying Chen, Joyce Y. Wong, Markus J. Buehler, and David L. Kaplan*

Elastomeric, robust, and biocompatible hydrogels are rare, while the need for these types of biomaterials in biomedical-related uses remains high. Here, a new family of genetically engineered silk–elastin-like proteins (SELPs) with encoded enzymatic crosslinking sites is developed for a new generation of stimuli-responsive yet robust hydrogels. Input into the designs is guided by simulation and realized via genetic engineering strategies. The avoidance of gamma irradiation or chemical crosslinking during gel fabrication, in lieu of an enzymatic process, expands the versatility of these new gels for the incorporation of labile proteins and cells. In the present study, the new SELP hydrogels offer sequence-dependent, reversible stimuli-responsive features. Their stiffness covers almost the full range of the elasticity of soft tissues. Further, physical modification of the silk domains provides a secondary control point to fine-tune mechanical stiffness while preserving stimuli-responsive features, with implications for a variety of biomedical material and device needs.

Dr. W. Huang, Dr. N. Dinjaski, Prof. Q. Wang,
Prof. X. Xia, Dr. Y. Chen, Prof. D. L. Kaplan
Department of Biomedical Engineering
Tufts University
4 Colby Street, Medford, MA 02155, USA
E-mail: david.kaplan@tufts.edu

A. Tarakanova, Prof. M. J. Buehler
Laboratory for Atomistic and Molecular Mechanics (LAMM)
Department of Civil and Environmental Engineering
Massachusetts Institute of Technology
Cambridge, MA 02139, USA

Prof. Q. Wang
Hubei Collaborative Innovation Center for Green
Transformation of Bio-Resource
College of Life Science
Hubei University
Wuhan 430062, P.R. China

Prof. X. Xia
State Key Laboratory of Microbial Metabolism
School of Life Sciences and Biotechnology
Shanghai Jiao Tong University
800 Dong-Chuan Road, Shanghai 200240, P.R. China

Prof. J. Y. Wong
Departments of Biomedical Engineering and Materials
Science and Engineering
Boston University
Boston, MA 02215, USA

DOI: 10.1002/adfm.201600236



1. Introduction

Hydrogels are 3D insoluble cross-linked polymer networks with an ability to retain a significant amount of aqueous medium within their porous structure. Historically, the designs have consisted primarily of relatively inert matrices, with tremendous impact on medicine, from contact lenses^[1] to the field of regenerative medicine.^[2] These materials are particularly attractive for tissue engineering,^[3,4] due to the high water content and the ability to mimic aspects of the 3D microenvironment of native tissue extracellular matrices (ECMs). However, these conventional hydrogels, once in the equilibrium swelling state, are limited to mimicking static environments and lack responses to endogenous environmental stimuli or natural signals from cells and tissues. These

features therefore restrict their applications in cell-mediated delivery of growth factors, swelling-controlled release of drugs in naturally low pH environment such as the gastro-intestinal tract, or detection of symptoms of disease as biological sensors.

Recent trends in hydrogel designs have evolved from static to dynamic, bio-responsive systems, to address broader biomedical needs for higher-performance materials. These hydrogels include stimuli-responsive hydrogels that can dramatically change their volume and other properties in response to environmental stimuli such as temperature, pH, and certain biological signals. The most extensively studied stimuli-responsive hydrogels are composed of synthetic polymers, such as temperature sensitive poly(N-isopropyl acrylamide),^[5] pH sensitive poly(acrylic acid),^[6] and their derivatives.^[7] While these studies demonstrated the potential of using stimuli-responsive hydrogels for artificial muscles,^[8] controlled drug delivery,^[9] smart diagnostics,^[10] optical systems,^[11] as well as actuated micropatterned materials and sensors,^[12] the polymers utilized to date are nondegradable *in vivo* and offer limited options in terms of responsive stimuli (e.g., temperature, pH).

In contrast, protein polymers provide a unique opportunity for the tunable design of such dynamic polymer systems, due to the genetic basis of sequence, molecular weight, and chirality control. Harnessing proteins to generate stimuli-responsive hydrogels based on protein folding–unfolding for biomedical

applications offers tremendous opportunities for fine tuning control, responses, and utility, such as for tissue regeneration scaffolds and controlled drug delivery devices.^[13] Further, compared to synthetic polymers, protein polymers are generally biocompatible and fully degradable in vivo, which is critical for many biomedical needs. The protein systems are also relatively easy to functionalize through diverse amino acid chemistries, or via the formation of well-defined supramolecular structures, such as β -sheets, α -helices, and β -turns. Moreover, with advances in genetic and protein engineering, these protein polymers can be designed *de novo* by permutation, combination, and with the addition of constituent modules to introduce functions, exploiting the modular nature of fibrous proteins. Therefore, protein polymers are ideal for designing new stimuli-responsive biomaterials which can undergo substantial changes in volume, shape, mesh size, mechanical stiffness, and optical transparency in response to specific target stimuli. As a starting point for these types of dynamic protein systems, the pioneering studies by Urry et al. on the coacervation phenomena of elastin-like proteins in solution provide a foundation for peptide sequence chemistry and stimuli-responses.^[14–16] These designs have been extended over the years by many groups. Self-assembled elastin copolymer micelles, nanoparticles, and micellar hydrogels have been used for targeted drug delivery and sensing.^[17,18] While these studies demonstrated the potential of using elastin or elastin block copolymers as dynamic delivery systems, the stimuli-responsive properties of these proteins were mostly appreciated when elastin like peptides were in solution. A few examples demonstrated that elastin coacervate can be chemically cross-linked via (hydroxymethyl) phosphines or physically cross-linked by gamma irradiation for temperature sensitive soft elastomeric matrix. However, the mechanical strength of those biomaterials is weak (less than 0.5 kPa and cannot hold their shape), and thus, refrains their uses for tissue engineering and bio-devices.^[19,20] Therefore, forming solid state, robust protein hydrogels with dynamic mechanical properties and fully translating the molecular level folding–unfolding of these proteins into macroscopic reversibly tunable physical properties remains challenging.

Here we report a new system for the design, synthesis, and fabrication of stimuli-responsive, robust, and tunable hydrogels, exploiting silk and elastin peptide motifs for the building blocks combined with enzymatic crosslinking to generate the solid state materials. Sequence features of our silk–elastin-like proteins (SELPs) include the elastin domain, GXGVP, as the soft domain providing elasticity and dynamic features, and the silk domain, GAGAGS, as the hard domain regulating the stimuli-responsive features and providing tunable mechanical stiffness by varying the degree of crystallinity (Figure S1a, Supporting Information). These new systems provide a number of novel features. (a) The generation of solid state responsive hydrogels from the SELPs was realized by horseradish peroxidase (HRP) catalyzed reactions from the tyrosine crosslinking sites encoded in the proteins (e.g., at the X position in the elastin domain). These elastin crosslinking networks played critical roles to translate molecular level protein folding–unfolding into macroscopic reversibly tunable physical properties (Figure S1b, Supporting Information). (b) The incorporation of modeling guided rational design of stimuli-responsive sequences. Here,

replica exchange molecular dynamics (REMD) simulations were integrated with the genetic engineering approaches for the rational design of elastin domains for hierarchical materials with predictable responses to specific environmental stimuli, such as temperature, pH, ionic strength, and biological triggers. In particular, sequence variants in the position “X” of the elastin domains that dominate further variants in material features were simulated to address the origin of dynamic material functions. (c) The combination of genetic engineering and molecular modeling provided a toolkit upon which to generate a broad range of stimuli-responsive systems to exploit toward new families of dynamic protein hydrogels. (d) The ability to fine tune the mechanical properties of the hydrogels via the silk domains modulated mechanical properties while preserving the stimuli-responsive features (Figure S1c, Supporting Information), in combination with the elastin domains related to sequence-specific responses.

The resultant SELP hydrogels exhibited significant swelling ratios as well as significant reversible changes in optical transparency, mechanical properties, and hydrogel pore size upon exposure to designed target stimuli. The development of these dynamic protein hydrogels based on SELPs suggests new possibilities for these hydrogels as biological structures in tissue regeneration and as vehicles for delivery. The insight gained will also allow enhanced understanding of structure–function relationships with protein designs, thus guiding genetic designs of dynamic hydrogels that respond predictably to virtually any desired environmental input to trigger changes in the material.

2. Results

2.1. Dynamic Design of Stimuli-Responsive SELPs Library

A library of SELPs consisting of 64 different SELP constructs with 12 different monomers and 3 different silk to elastin ratios was biosynthesized via seamless cloning strategies as described previously^[18,21] and purified via inverse temperature transition cycling (Figure S2, Supporting Information) with an average yield of purified protein of about 1 g L⁻¹. The purity and molecular weight of the proteins were checked by sodium dodecyl sulfate polyacrylamide gel electrophoresis (SDS-PAGE) (Figure S3, Supporting Information). Each individual SELP construct was named as S_nE_{mX}, based on both the silk to elastin ratio n:m and its characteristic amino acid “X” in the elastin blocks. The silk and elastin peptide motifs used in our SELP library are shown in Figure S4 (Supporting Information), with silk blocks serving as the mechanical reinforcement motifs and elastin blocks serving as the stimuli-responsive motifs. Different amino acids (C, F, G, Y, I, E, K, RGYSLG) were employed in the elastin domains at the second amino acid position of the fifth elastin block in each SELP monomer to expand the diversity of the library. This position “X” amino acid in elastin domains was designed to control chain dynamics and the intermolecular or intramolecular interactions of SELP molecules in aqueous environments, in order to control the dynamic functions of the SELPs, via altering the hydrophobicity and surface charge of the “X” residue.^[15,16] Stimuli that were

selected to trigger the reversible conformational transitions in the elastin domains were classified into three categories: (1) physical stimuli, such as temperature, electric field, light; (2) chemical stimuli, such as pH, redox state, ionic strength; and (3) biological stimuli, such as enzymatic triggers, glucose. By varying position "X" amino acid in the elastin blocks, SELPs can be designed to predictably respond to a single stimulus in each category, or exhibit multistimuli-responsive properties that simultaneously respond to more than one stimulus (**Figure 1a–c**). The SELPs with the hydrophobic residues at position "X," such as C and F, responded to temperature changes and exhibited inverse temperature transitions as the temperature was raised through the transition temperature (Figure 1a). The SELPs with the negatively charged residues at position "X," such as E, exhibited inverse temperature transitions at 34 °C in pH4 phosphate–citrate buffer, but no response in water (Figure 1b), suggesting that this SELP responds to pH changes in the temperature window above 34 °C. The SELPs with the biological recognition site as position "X" residues, such as RGYSLG that can be recognized by protein kinase for phosphorylation,^[22] exhibited elevated inverse transition temperature once the sequences were phosphorylated (Figure 1c). These results demonstrate that SELPs can be rationally designed to be responsive to a specific stimulus. The insight gained provided a starting base for utilizing the SELP library for the fabrication of dynamic hydrogels.

To study the molecular mechanisms underlying the stimuli-responsive features of the elastin domains, molecular dynamics (MD) simulations were used to identify temperature transitions associated with a single peptide, employing the replica

exchange molecular dynamics paradigm for enhanced sampling. We considered two tri-block peptides, with amino acid sequence (GVGVP)(GXGVP)(GVGVP), where the X residue was chosen to be valine (V) or lysine (K) (Figure 1d–g). We observed a transition in the X = V sequence which was characterized by structural folding of the peptide, associated with a hydrophobic collapse thought to be responsible for elastin's inverse temperature transition (Figure 1d,e). By substituting the lysine residue (X = K), we showed that this structural transition could be suppressed (Figure 1f,g), demonstrating proof of concept of the tunability of elastin domains at the molecular scale.

2.2. Fabrication of SELP Smart Hydrogels and Structural Characterization

In order to translate protein chain folding–unfolding at the molecular level into reversible macroscopic, solid-state material physical properties changes, the elastin domains were cross-linked to fabricate stimuli-responsive SELP hydrogels (**Figure 2**). The SELPs that were designed with a tyrosine residue in the "X" position of the elastin blocks, named S_nE_{8Y} and S₂E_{8R}, were selected as proof-of-concept examples and cross-linked to form hydrogels via an aqueous, enzymatic process based on HRP-mediated redox reaction^[23] (Figure 2a). In brief, S_nE_{8Y} or S₂E_{8R} were dissolved in deionized water at 4 °C overnight to obtain a homogenous solution; then the addition of H₂O₂ in the presence of HRP resulted in the formation of inter and intramolecular covalent crosslinks between

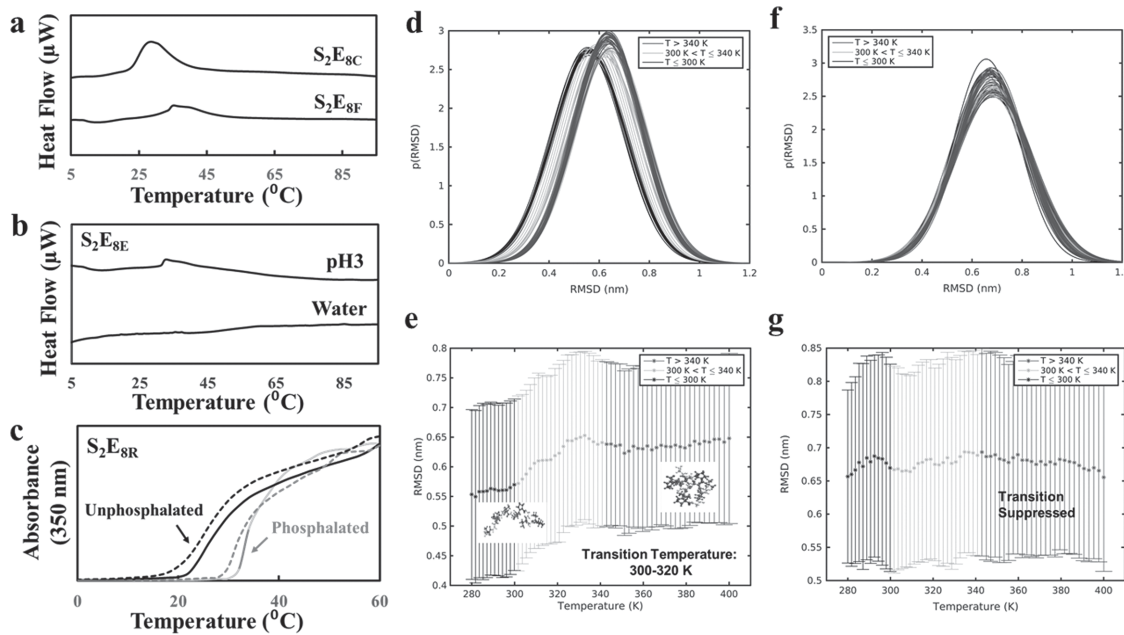


Figure 1. SELP dynamic hydrogel designs inspired by the nature of the environmental stimulus. a) SELPs respond to temperature, a physical stimulus, exemplified by S₂E_{8C} and S₂E_{8F}. b) SELPs respond to pH, a chemical stimulus, exemplified by S₂E_{8E}. c) SELPs respond to phosphorylation, a biological stimulus, exemplified by S₂E_{8R}. d) Gaussian fits to the distribution of structures characterized by root mean square deviation (RMSD) from extended linear conformation at a range of temperatures for the X = V sequence. e) Mean RMSD values for the X = V sequence indicating a transition from extended to folded conformations. f) Gaussian fits to the distribution of structures characterized by root mean square deviation (RMSD) from extended linear conformation at a range of temperatures for the X = K sequence. g) Mean RMSD values for the X = K sequence suggesting a suppressed transition.

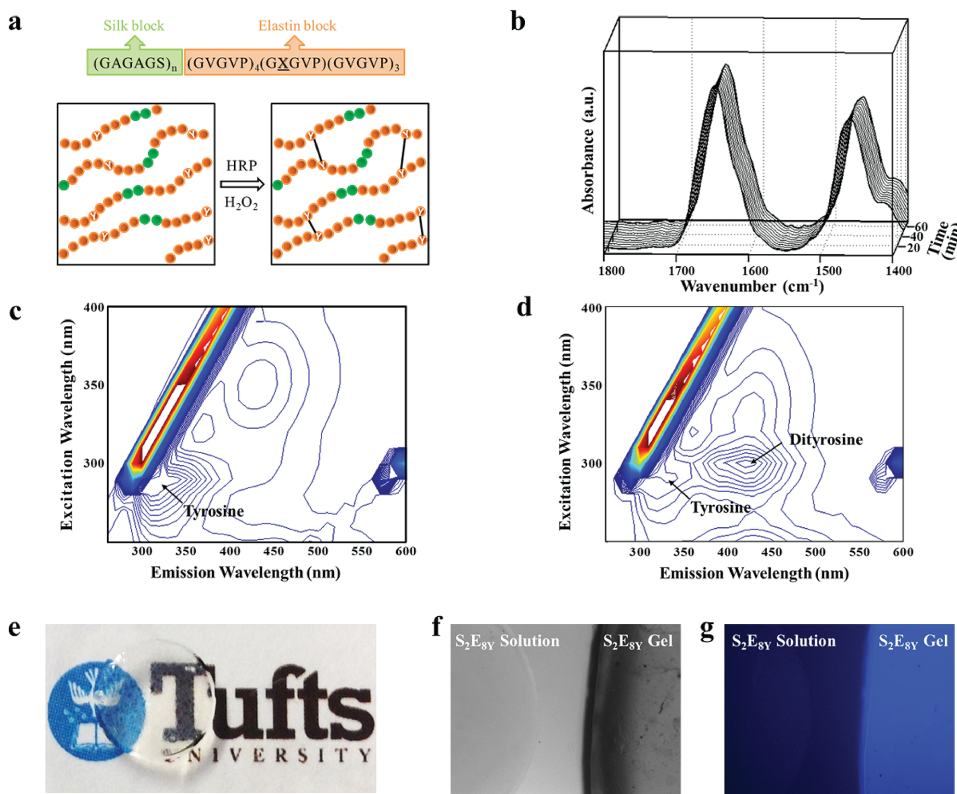


Figure 2. SELP dynamic hydrogel schematics and structural characterization. a) Mechanism of HRP-mediated SELP gelation: the formation of inter and intramolecular covalent crosslinks (black lines) between elastin blocks allows for chain extension for stimuli responsive hydrogels. b) Real-time FTIR spectra of S_2E_{8R} during gelation suggest the formation of the SELP hydrogel is not based on β -sheet crosslinks. Fluorescence excitation–emission spectra of c) S_2E_{8Y} solution and d) S_2E_{8Y} hydrogel confirmed the formation of dityrosines between the elastin blocks. e) The resultant S_2E_{8Y} hydrogels are optically clear and f,g) exhibit blue fluorescence when irradiated with UV, a feature not present in the precursor protein solution.

tyrosine residues, leading to the formation of a stable, highly elastic hydrogel. These elastin networks, represented by the black solid lines in Figure 2a, are essential for dynamic SELP hydrogels.

The formation of elastin networks based on dityrosine bonds and hydrogel secondary structure during gelation was assessed by real-time Fourier transform infrared spectroscopy (FTIR) and by fluorescence spectroscopy. Real-time FTIR spectra collected during S_2E_{8R} gelation (Figure 2b) showed no significant structural changes during the gelation process, especially in the 1624 cm^{-1} absorbance region for the presence of anti-parallel β -sheets.^[24] This result suggested that the enzymatic crosslinking gelation mechanism was not based on β -sheet formation, which would have constrained long range protein chain displacements due to the crystal formation.^[25] Fluorescence spectroscopy confirmed dityrosine formation by comparison of the fluorescence excitation–emission matrix for the SELP solutions (Figure 2c) and the fully formed hydrogels (Figure 2d). These data show a distinct shift in the fluorescence maxima from the solution with an excitation of 290 nm and an emission of 350 nm to the hydrogel with a peak excitation of 300 nm with an emission at 425 nm . The shift in fluorescence indicates the formation of dityrosine covalent crosslinks during gelation.^[4] Furthermore, enzymatic crosslinking of S_2E_{8Y} resulted in the formation of optically clear hydrogels (Figure 2e). The resultant

hydrogel also emitted blue fluorescence when irradiated under UV due to the presence of the dityrosines, a feature not found in the precursor solution (Figure 2f,g).

2.3. Tunable Responsive Properties of SELP Dynamic Hydrogels

In order to harness the stimuli-responsive properties of the SELP hydrogels, S_2E_{8Y} , S_4E_{8Y} , and S_2E_{8R} with concentrations from 2% to 20% were studied upon exposure to specific stimuli. Prior to the stimuli-response studies, all the SELP hydrogels were extensively extracted with deionized water to remove residual reactants and then equilibrated in deionized water, 1 M NaCl or phosphate buffered saline (PBS) buffer for 24 h at 4°C . The equilibrium swelling ratio of the hydrogels in deionized water was between 100% and 200% (Figure S5, Supporting Information), which decreased on increasing the hydrogel concentration or the silk-to-elastin ratio, due to increased crosslinking or structural support from the silk domains. The deswelling behavior of the hydrogels in PBS buffer varied with the amino acid in the “X” position: S_nE_{8Y} hydrogels maintained constant weight with a degree of swelling about 100% in PBS, while S_2E_{8R} significantly contracted to 50% of the original weight due to osmotic pressure induced by electrostatic shielding around charged arginine residues

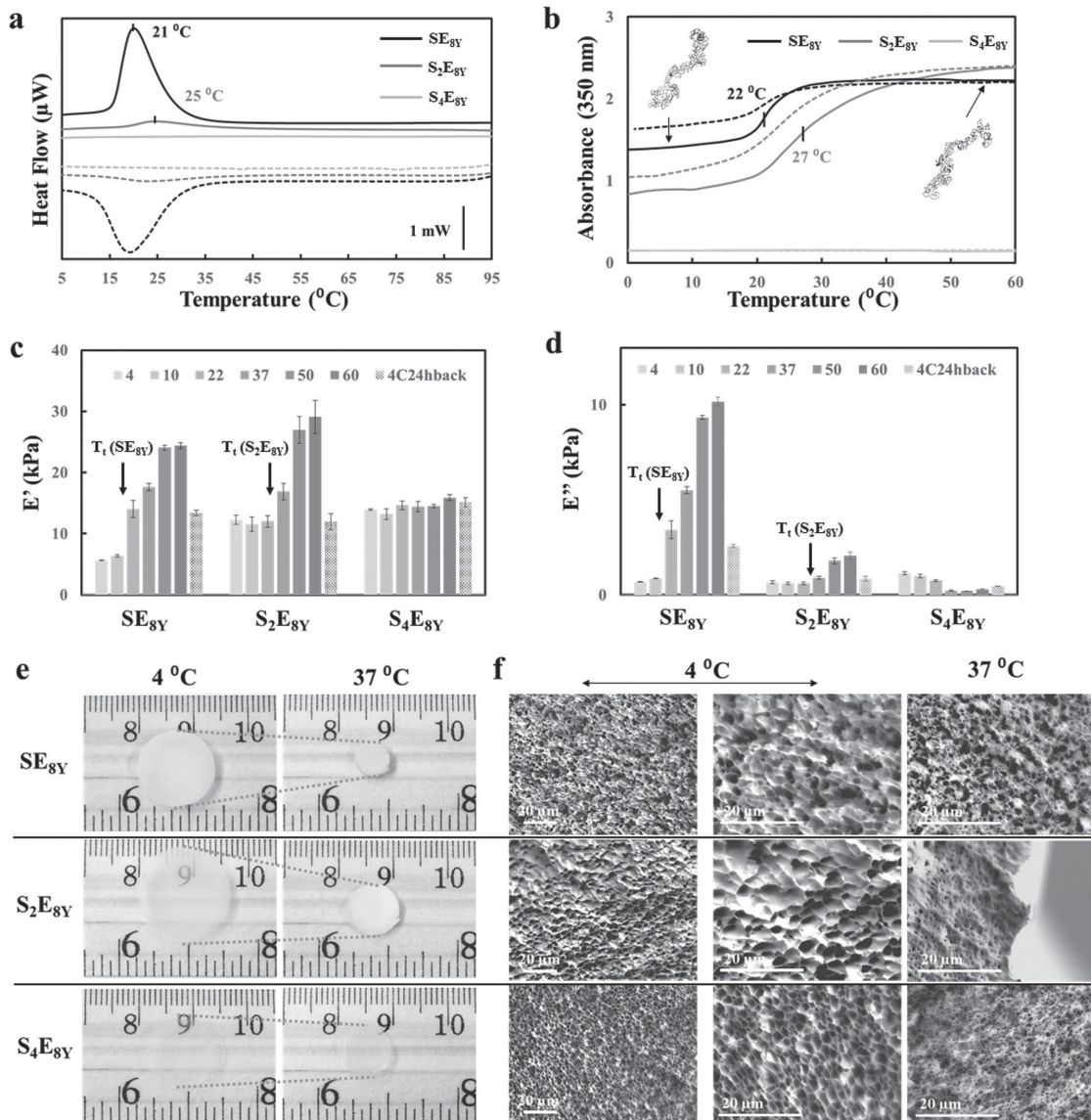


Figure 3. Thermoresponse of SELP dynamic hydrogels. LCST of 2% SELP hydrogels determined by a) DSC heat flow versus temperature curves and b) turbidity, suggesting silk-to-elastin ratio governed thermoresponses. Keys: SE_{8Y} (black curves), S₂E_{8Y} (dark gray curves), and S₄E_{8Y} hydrogel (light gray curves). The heating (solid lines) and cooling (dashed lines) rate was 2 °C min⁻¹. Viscoelastic properties, including c) storage modulus and d) loss modulus of 10% SELP hydrogels measured in water at 4, 10, 22, 37, 50, and 60 °C by DMA suggesting an increase of hydrogel stiffness and viscosity when the temperature was raised above the LCST for the SE_{8Y} and S₂E_{8Y} hydrogels. e) Optical and f) SEM images showing the size and micromorphology differences of 2% SELP hydrogels in swollen states at 4 °C (<LCST) and in the contracted states at 37 °C (>LCST) in deionized water.

(Figure S6, Supporting Information). The physical stimuli responsive properties of SELP hydrogels were investigated via thermodynamic, optical, mechanical, and morphological approaches. The thermoresponsive features of SE_{8Y}, S₂E_{8Y}, and S₄E_{8Y} hydrogels with different silk-to-elastin ratios were characterized by differential scanning calorimetry (DSC), UV-vis spectrophotometry, dynamic mechanical analysis (DMA), optical imaging, and scanning electron microscopy (SEM) (**Figure 3**). DSC heat flow curves showed that 2% SE_{8Y} and S₂E_{8Y} hydrogels exhibited lower critical solution temperatures (LCSTs) at 21 and 25 °C, respectively, while the S₄E_{8Y} hydrogel did not display a thermoresponse (Figure 3a). The exothermic

transition during cooling and the sharp endothermic transitions in the DSC rescans during heating (Figure S7, Supporting Information) suggested a reversible temperature transition in SE_{8Y} and S₂E_{8Y} hydrogels. Turbidity profiles of 2% SE_{8Y}, S₂E_{8Y}, and S₄E_{8Y} hydrogels confirmed the reversible thermoresponse of the SE_{8Y} and S₂E_{8Y} hydrogels, and the static nature of the S₄E_{8Y} hydrogel (Figure 3b). The optical absorbance from 300 to 800 nm at 4 and 60 °C also suggested that these SELP hydrogels changed in optical transparency upon exposure to thermal triggers: the optical profiles of SELP hydrogels showed that the 2% SELP hydrogels were almost clear with negligible absorbance above 500 nm at 4 °C, except for SE_{8Y}, and when they

were exposed to an environment with a temperature above their LCSTs the optical absorbance increased and became more opaque (Figure S8, Supporting Information). Viscoelastic properties, including the storage modulus (Figure 3c) and the loss modulus (Figure 3d) of 10% SELP hydrogels measured in water at 4, 10, 22, 37, 50, and 60 °C by DMA, showed an increase of hydrogel stiffness and viscosity when the temperature was above the LCST for the SE_{8Y} and S₂E_{8Y} hydrogels. No significant change in storage modulus, but a decrease of loss modulus around 37 °C, was observed for the S₄E_{8Y} hydrogels, suggesting that hydrophobic hydration^[15] of the elastin domain still occurred in S₄E_{8Y} which led to a less viscose hydrogel matrix at higher temperatures. When the hydrogels were equilibrated back to 4 °C after exposure to thermal triggers, the storage and loss modulus of SE_{8Y} was higher than its original values suggesting a semi-reversible response, while the storage and loss modulus of S₂E_{8Y} and S₄E_{8Y} changed back to their original values suggesting the silk served as a structural support and facilitated the reversible mechanical response. Optical images (Figure 3e) showed that the 2% SELP hydrogels had a large thermoresponsive equilibrium deswelling ratio, except for S₄E_{8Y}. Upon exposure to thermal triggers above the LCST, 10% SELP hydrogels contracted to 13%, 64%, and 84% of their original weight for SE_{8Y}, S₂E_{8Y}, and S₄E_{8Y}, respectively, depending on the silk-to-elastin ratio (Figure S9, Supporting Information). The SEM images (Figure 3f) showed that freeze-dried SELP hydrogels were porous; in swollen states at 4 °C (<LCST) the average pore sizes were about 4 μm, and in the contracted states at 37 °C (>LCST) the average pore size was about 1 μm in deionized water. In summary, SE_{8Y} and S₂E_{8Y} hydrogels showed large responsive deswelling ratios as well as significant reversible changes in optical transparency, viscoelastic properties, and micromorphology in response to environmental temperature changes across the LCST; while S₄E_{8Y} exhibited no significant thermoresponse. These results suggested that the stimuli responsive properties of the SELP hydrogels were tunable by adjusting the silk-to-elastin ratios.

The chemical stimuli responsive properties of SELP hydrogels were also investigated via thermodynamic, optical, mechanical, and morphological approaches. In particular, the ionic strength responsive features of SE_{8Y}, S₂E_{8Y}, S₄E_{8Y}, and S₂E_{8R} hydrogels with various silk-to-elastin ratios or different "X" position amino acids were characterized (Figure 4). DSC heat flow versus temperature curves showed that changes in solvent chemical potential caused a shift in the temperature of the inverse temperature transition^[20] (Figure 4a,b); when submerged in 1 M NaCl, the LCSTs of 2% SE_{8Y}, S₂E_{8Y}, S₄E_{8Y}, and S₂E_{8R} hydrogels were 12, 18, 27, and 16 °C, respectively; while when submerged in deionized water, the LCSTs of 2% SE_{8Y}, S₂E_{8Y}, and S₂E_{8R} were 21, 25, and 26 °C, respectively, with no LCST observed for the S₄E_{8Y}. These results suggested that the SELP hydrogels exhibited significantly decreased LCST in a solvent with high ionic strength, and thus responded to the changes of solvent chemical potential in a well-defined temperature window. Particularly, SE_{8Y}, S₂E_{8Y}, S₄E_{8Y}, and S₂E_{8R} responded to the changes in solvent from deionized water to 1 M NaCl in the temperature ranges 12–21, 18–25, above 27 and 16–26 °C, respectively. The storage modulus of 10% SELP hydrogels measured in water and 1 M NaCl at 4, 10, 22, and 37 °C

by DMA further demonstrated that the hydrogels responded to the changes in solvent based on two mechanisms: (a) shifting the LCST or (b) deswelling, depending on the silk-to-elastin ratio and the "X" residue in the elastin block (Figure 4c,d). The DMA showed an increase stiffness for the 10% SE_{8Y} hydrogel at 10 °C, and an increase stiffness of the 10% S₂E_{8Y} and S₄E_{8Y} hydrogels at 22 °C and above; while the 10% S₂E_{8R} hydrogel responded to solvent changes at all temperatures because of its deswelling properties in 1 M NaCl. Optical images (Figure 4e) showed that upon exposure to chemical or physical triggers, the S₂E_{8R} hydrogels exhibited significant contraction. The 10% S₂E_{8R} hydrogels contracted to about 34% of the original weight when exposed to a temperature above the LCST, and 65% when submerged in 1 M NaCl (Figure S10, Supporting Information). SEM images (Figure 4f) showed that freeze-dried S₂E_{8R} hydrogels were porous in deionized water with the average pore size being about 6 μm in the swollen state at 4 °C (<LCST) and about 2 μm in contracted state at 37 °C (>LCST); when submerged in 1 M NaCl the micromorphology of S₂E_{8R} hydrogels changed to a layered structure with the average layer-to-layer distance of about 10 μm in the swollen state at 4 °C (<LCST) and less than 1 μm in the contracted state at 37 °C (>LCST). In summary, the SE_{8Y}, S₂E_{8Y}, S₄E_{8Y}, and S₂E_{8R} hydrogels showed large responsive deswelling ratios as well as significant reversible changes in viscoelastic properties and micromorphology in response to changes in ionic strength in well-defined temperature windows, depending on silk-to-elastin ratio or the "X" residue in the elastin block.

2.4. Tunable Mechanical Properties of SELP Hydrogels

Matching mechanical properties of biomaterials to native tissue extracellular matrix is an important consideration during the selection of biomaterials for tissue engineering and regenerative medicine.^[4,26] In order to fine tune the stiffness of the SELP hydrogels, SE_{8Y}, S₂E_{8Y}, S₄E_{8Y}, and S₂E_{8R} from 2% to 20% were studied (Figure 5). The Young's moduli in aqueous environments demonstrated a wide range of stiffnesses was achievable by adjusting the silk-to-elastin ratio or the hydrogel concentration (Figure 5a). The hydrogel stiffness could also be further reinforced by the formation of β-sheets in the silk blocks via treatment with methanol (Figure 5b). Based on the concentrations and conditions studied, stiffness values between 1 and 64 kPa were obtained, where 2% SE_{8Y} hydrogels had the lowest stiffness and the 20% S₄E_{8Y} methanol-treated hydrogel had the highest stiffness. These values cover almost the full range of the elasticity of soft tissues.^[27] FTIR absorbance at 1624 cm⁻¹ confirmed that β-sheets were formed in the SELP hydrogels after treatment with methanol (Figure 5c), and these β-sheet crystals served as structural support to increase the stiffness of the hydrogels. The stimuli-responsive properties of the SELP hydrogels before and after methanol treatment were also investigated. In particular, the 10% SE_{8Y} hydrogels with and without β-sheets showed similar thermoresponsive properties; the treated hydrogels had almost the same LCST as the untreated (noncrystalline) hydrogel, while a smaller degree of contraction was found for the treated (crystalline) hydrogel upon exposure to temperature triggers due to the constraints of long range

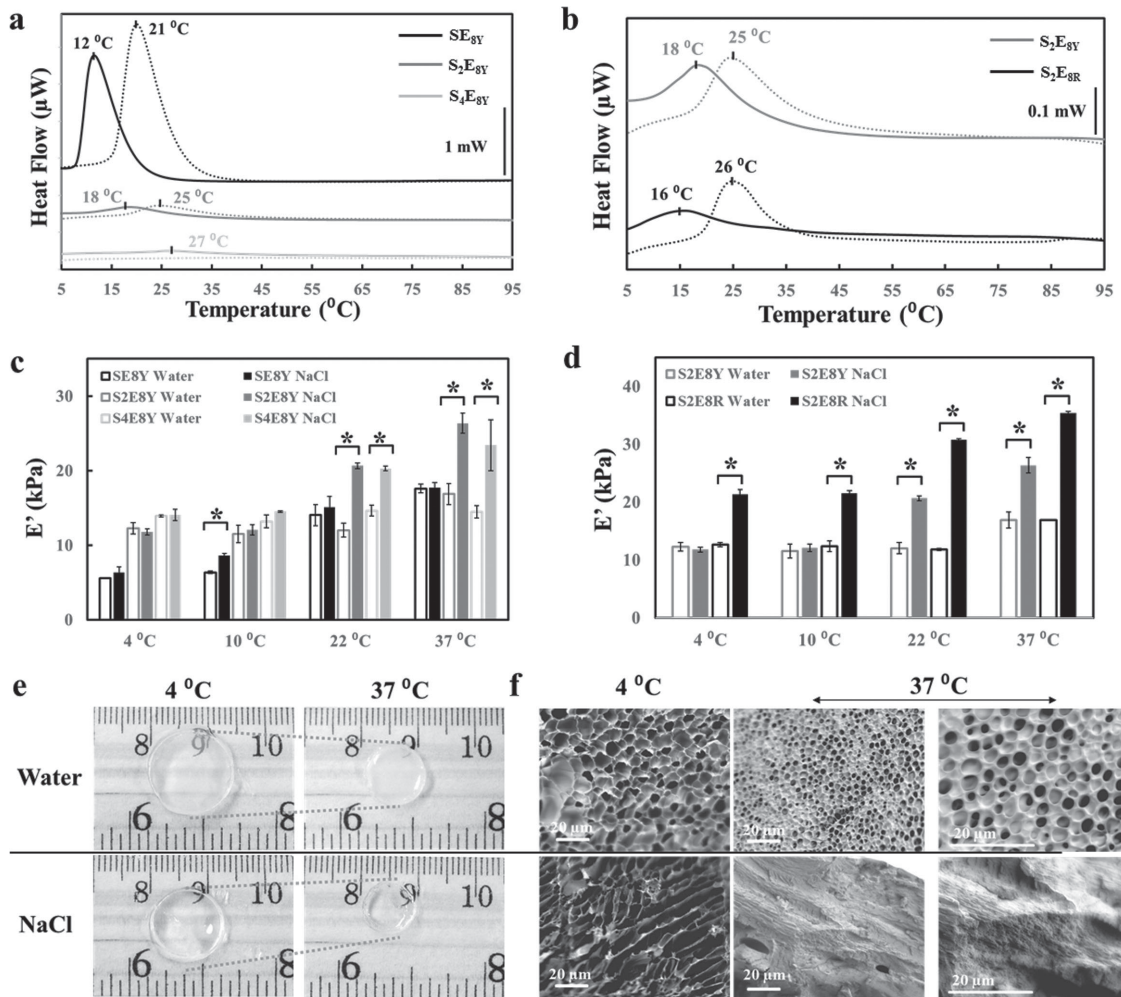


Figure 4. Ionic strength responsive properties of SELP dynamic hydrogels. LCST was determined by DSC heat flow versus temperature curves for 2% SELPs, suggesting a) a silk-to-elastin ratio and b) the position of the “X” residue governed the chemical response. Keys: SE_{8Y} (black curves), S₂E_{8Y} (dark gray curves), S₄E_{8Y} hydrogel (light gray curves), and S₂E_{8R} (black curves) in 1 M NaCl (solid curves) or deionized water (dashed curves). Storage modulus of 10% SELP hydrogels was determined by DMA at 4, 10, 22, and 37 °C, suggesting the response to ionic strength depended on c) silk-to-elastin ratio and d) position “X” residue in elastin block. e) Optical and f) SEM images showing the size and micromorphology of 2% S₂E_{8R} hydrogel samples in swollen states at 4 °C (<LCST) and in contracted states at 37 °C (>LCST) in deionized water and 1 M NaCl.

protein chain displacements induced by the β -sheet crystals (e.g., physical crosslinks) (Figure 5d).

2.5. Biocompatibility of SELP Hydrogels

Apart from desirable material properties, low cytotoxicity and good mammalian cell adhesion for biomaterials are important features, thus human mesenchymal stem cell (hMSCs) were grown on hydrogel surfaces and assessed by live/dead staining. Fluorescent imaging of live/dead staining confirmed that the hMSCs seeded on the SELP hydrogels showed similar adhesion as the control tissue culture plate (TCP) surface and supported cell growth and proliferation for 2 weeks (Figure 5e). An elongated morphology of hMSCs was observed on all tested surfaces after 14 d suggesting a healthy growth of hMSCs and minimal cytotoxicity of the SELP hydrogels.

3. Discussion

Protein polymers provide a uniquely tunable family of functional biomaterials for biomedical engineering, yet creating stimuli-responsive protein hydrogels with dynamic physical properties remains challenging. This limitation is due to a limited understanding of sequence–function relationships for the rational design of protein polymers, as well as the limited methods to translate the protein folding–unfolding upon triggers at molecular level into the reversible and tunable physical property changes at macroscopic scale. To overcome these gaps between dynamic protein molecules and dynamic actuating biomaterials, a protein material system to systematically study and develop dynamic protein hydrogels is needed, for both fundamental insights and for potential biomedical applications.

The present work demonstrated the design and fabrication of a new family of biocompatible, biodegradable, elastomeric,

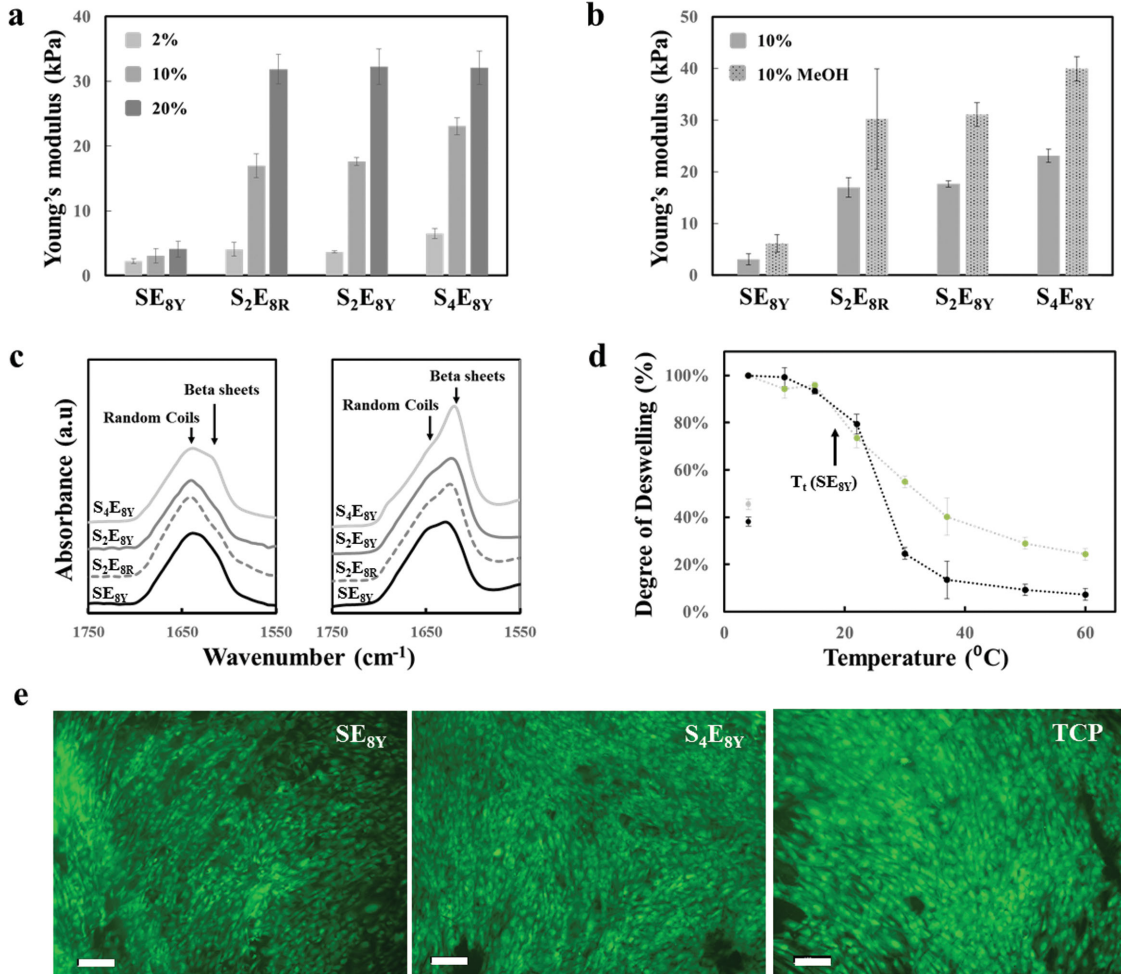


Figure 5. Tunable mechanical properties and biocompatibility of SELP hydrogels. a) Young's moduli of SELP hydrogels as a function of silk-to-elastin ratio and hydrogel concentration measured in water at 4 °C, demonstrating the wide range of stiffnesses achievable. b) Young's moduli of 10% SELP hydrogels before and after methanol treatment measured in water at 4 °C, demonstrating tunable stiffness achieved by varying β-sheet content. c) FTIR spectra of SELP hydrogels before (left) and after (right) methanol treatment, showing the increase of hydrogel stiffness originated from β-sheet formation and the degree of crystallinity induced was positively related to the silk-to-elastin ratio. d) The responsive feature of SELP hydrogels preserved upon β-sheet formation, exemplified by SE_{8Y}. e) Human mesenchymal stem cell interactions on SELP hydrogel surfaces: live (green) and dead (red) cell staining on SE_{8Y} (left), S₄E_{8Y} hydrogels (middle), and TCP (right) over a 14 d period. Scale bars are 100 μm.

stimuli-responsive protein hydrogels for use in tissue engineering and regenerative medicine, exploiting silk and elastin peptide motifs as the building blocks. Genetic engineering strategies were used to design a SELP library consisting of 64 different SELP constructs with 12 different monomer designs and 3 different silk to elastin ratios, inspired by prior solution studies of the coacervation phenomena of ELP and ELP copolymers. Replica exchange molecular dynamics (REMD) simulations were also integrated with the experimental studies to guide the rational design of elastin domains for new complex hierarchical materials with predictable responses to specific environmental stimuli, such as temperature, pH, ionic strength, and biological triggers. To fabricate dynamic hydrogels, the SELPs were designed with a tyrosine residue in the “X” position of the elastin blocks to form hydrogels via an enzymatic crosslinking reaction based on HRP. The fabrication procedure for SELP dynamic hydrogels is an all aqueous

method and the resulting hydrogels SE_{8Y} and S₂E_{8Y} showed large responsive deswelling ratios as well as significant reversible changes in optical transparency, viscoelastic properties, and micromorphology in responding to an environmental temperature change across the LCST. In contrast, S₄E_{8Y} exhibited no significant thermoresponse. These results suggested that the stimuli responsive properties of SELP hydrogels were tunable by adjusting the silk-to-elastin ratio of SELP molecules. SE_{8Y}, S₂E_{8Y}, S₄E_{8Y}, and S₂E_{8R} hydrogels also showed large responsive deswelling ratios as well as significant reversible changes in viscoelastic properties and micromorphology in response to changes in ionic strength over well-defined temperature windows, depending on silk-to-elastin ratio or the “X” residue in the elastin block. These results demonstrated the importance of the guest amino acid residue in elastin blocks and silk-to-elastin ratio for the rational design of responsive SELP dynamic hydrogels.

The mechanical properties of hydrogels play important roles in modulating cell–matrix interactions, as well as regulating a variety of biological processes, such as cell proliferation and differentiation. In order to fine tune the stiffness of these new SELP hydrogels, S_E_{8Y}, S₂E_{8Y}, S₄E_{8Y}, and S₂E_{8R} at various concentrations from 2% to 20% were subjected to methanol treatment to induce β -sheet formation for reinforced structures. Stiffness values between 1 and 64 kPa, which cover almost the full range of the elasticity of soft tissues, were obtained by adjusting the silk-to-elastin ratio or the hydrogel concentration. Apart from these desirable material properties, the SELP hydrogels supported hMSC survival and adhesion, suggesting minimal cytotoxicity as potential biomaterials. Additionally, the ability to trigger the responsive properties of SELP hydrogels suggests utility for delivery and release of bioactive molecules for dynamic biomaterial needs.

Molecular dynamics simulations provided insights into the mechanisms behind the transition capabilities of the elastin domains and confirmed a molecular-scale dependence on sequence, illustrated in a suppressed temperature transition upon changing the X residue within the elastin block. These results suggest that variable intramolecular structural folding at least partially contributes to the tunability of elastin-based protein systems. The effect is scaled up in large protein polymer systems such as the SELPs presented in this work. Sequence change may force a molecular-level suppression of this temperature-driven folding behavior, effectively quelling or modifying the macroscale transitions.

4. Conclusion

In conclusion, a generic design approach for dynamic, fully degradable, and biocompatible protein hydrogels was developed and used for the construction of a variety of dynamic SELP hydrogels. A number of studies have demonstrated the potential of using elastin or elastin block copolymers as dynamic drug delivery systems, but the stimuli-responsive properties of these proteins were exploited only in the solution state. In the present study dynamic properties of SELPs were fully translated from molecular level folding–unfolding informed by both modeling and experimental inputs into macroscopic reversibly tunable solid state materials. The hydrogel fabrication process included a facile approach to obtain functional elastomeric dynamic protein hydrogels via an all aqueous, enzymatic crosslinking method. Select SELP hydrogels exhibited a range of dynamic physical properties including large responsive swelling ratios as well as significant reversible changes in optical transparency, mechanical properties, and micromorphology upon exposure to designed target stimuli, dependent on the silk-to-elastin ratio or the guest amino acid residue designed in the elastin domain. Further, physical modification of the silk domains via β -sheet formation provided a secondary control point to fine-tune mechanical stiffness to match ECMs while preserving stimuli-responsive features. Overall, this work systematically studies the sequence–structure–process–property relationships for producing dynamic biomaterials. These results will be useful to guide future library designs with specific targeted properties, leading to new opportunities in biomimetics, biomaterials, and tissue engineering.

5. Experimental Section

Synthesis of Polymers: SELP expression plasmids were constructed using our previously established procedures.^[18,21] Briefly, DNA sequences were designed to encode the SELP sequences: S_E_{8X} [(GAGAGS)(GVGVP)₄(GYGVP)(GVGVP)₃], S₂E_{8X} [(GAGAGS)₂(GVGVP)₄(GXGVP)(GVGVP)₃], and S₄E_{8X} [(GAGAGS)₄(GVGVP)₄(GYGVP)(GVGVP)₃], where X was C, E, F, G, K, I, Y or RGYSLG. The monomer DNA sequences were cloned into Eco-RV site of the vector pUC57 from GenScript (Piscataway, NJ). The *Ban*I restriction sites were designed to flank each of the monomer oligonucleotide sequences. The monomer DNA sequences were liberated by digesting the pUC57 derivatives with *Ban*I (New England Biolabs, Beverly, MA), isolated by preparative gel electrophoresis, and purified using the QIAquick Gel Extraction kit (Qiagen, Valencia, CA). The purified monomer DNA was then self-ligated with T4 DNA ligase (New England Biolabs, Beverly, MA) for 8 h at 16 °C to yield DNA multimers. The SELP multimer genes were inserted in the tailor-made expression vector, pET-19b3, and expressed under the T7 promoter in *Escherichia coli* strain BL21Star (DE3) (Invitrogen, Carlsbad, CA). The recombinant strains were grown at 37 °C in 500 mL flasks containing 100 mL of Luria-Bertani medium for overnight culture in a shaking incubator at 250 rpm. A 100 mL seeding culture was transferred to 2 L of yeast extract medium and cultured at 37 °C pH 6.8 using a New Brunswick BioFlo 3000 bioreactor (New Brunswick Scientific, NJ). Cells were induced with 1 × 10⁻³ M isopropyl- β -D-thiogalactopyranoside (Sigma-Aldrich, St. Louis, MO) when the optical density at 600 nm reached ≈10. At 6 h after induction cells were harvested by centrifugation at 8000 rpm for 15 min at 4 °C. SELPs were purified using the inverse temperature cycling method (Figure S2, Supporting Information). Briefly, the bacterial pellet was resuspended in PBS with lysozyme, and the cells were disrupted by sonication on ice. The cell lysate was cleared by centrifugation at 8000 rpm for 15 min at 4 °C, and then the supernatant containing SELP was diluted by 2X TN buffer, incubated at 65 °C for 2 h, and warm centrifuged at 5000 rpm for 3 min at 40 °C. The supernatant was then discarded, and the pellet containing SELP was recovered by deionized water at 4 °C followed by another cold spin at 8000 rpm for 15 min at 4 °C. The supernatant containing the purified SELPs was dialyzed (MWCO 3.5 kDa) against deionized water for 2 d. The yield of SELP was ≈1 g of purified protein from per liter of culture medium. The purity of the proteins was monitored via SDS-PAGE (Figure S3, Supporting Information), and the molecular weights of the proteins were determined by MALDI-TOF (Bruker Corporation, Billerica, MA).

Preparation of Enzymatically Cross-Linked SELP Hydrogels: The lyophilized SELP powder was dissolved in deionized water at 4 °C for 4 h to form an SELP stock solution. HRP type VI lyophilized powder (Sigma-Aldrich, St. Louis, MO) was mixed with deionized water to form a 40 mg mL⁻¹ HRP stock solution with a concentration of 10 000 U mL⁻¹. To fabricate a 10% SELP hydrogel, 6 μ L of HRP stock solution was added to 100 μ L 10% SELP stock solution, and then the crosslinking reaction of SELP was initiated by adding 0.2 μ L of 30 wt% H₂O₂ solution to the SELP and HRP mixture with a final H₂O₂ concentration of 18 × 10⁻³ M. The reaction mixture was mixed by gentle pipetting prior to gelation. The enzymatically cross-linked SELP hydrogels were formed by incubation at 4 °C overnight. To fabricate 2% and 20% SELP hydrogels, the same SELP:HRP:H₂O₂ ratio and crosslinking reaction protocol was used for SELP gelation. An inversion test was used to qualitatively characterize the gelation time for each SELP hydrogel.

Fluorescence Spectroscopy: The excitation–emission spectra of 2% SELP solution and hydrogel were recorded using a Hitachi F4500 Spectrofluorometer (Hitachi, Schaumburg, IL). The 2% SELP solution was pipetted into a 2 mm path length fluorescence cuvette (Hellma USA, Plainview, NY), and the excitation–emission spectra were collected from 260 to 600 nm in 10 nm increments at an intensity of 700 V using a 5 nm slit width to avoid saturation. To measure the excitation–emission spectra of SELP hydrogel, 2% SELP solution with HRP and H₂O₂ was mixed and pipetted into the fluorescence cuvette, allowed to gel at 4 °C overnight, and the excitation–emission spectrum of the hydrogel was collected by the spectrofluorimeter. The excitation–emission spectra

were then processed to subtract background fluorescence from the solvent and cuvette. Fluorescence images of SELP solution and hydrogel were acquired on a Leica DM IL fluorescence microscope (Leica Microsystems Inc., Buffalo Grove, IL) with an A4S DAPI filter. Images were processed using both Leica Application Suite V3 and ImageJ.

Fourier Transform Infrared Spectroscopy: FTIR was carried out on a Jasco (Japan) FT/IR-6200 spectrometer with a deuterated triglycine sulfate detector. To capture the secondary structure changes during SELP sol-gel transition, real-time FTIR was performed in transmission mode with a demountable FTIR liquid cell with BaF₂ windows (Pike Tech., Madison, WI). The 2% SELP D₂O solution with HRP and H₂O₂ was mixed and pipetted into the FTIR liquid cell, and the real-time FTIR absorbance spectra were obtained every 5 min till the gelation reaction completed. To access the secondary structure of SELP hydrogels, ATR-FTIR was performed in ATR mode with a horizontal MIRacle ATR attachment (fadison, WI). The 10% SELP hydrogels were fabricated in D₂O, and FTIR absorbance spectra of the SELP hydrogels before and after methanol treatment were obtained. For each measurement, 32 scans were co-added with a resolution of 4.0 cm⁻¹, and the wavenumbers ranged from 400 to 4000 cm⁻¹. The background spectra were taken under the same conditions and subtracted from the sample scans.

Differential Scanning Calorimetry: DSC measurements were performed with Nano DSC II Model 6100 (Calorimetry Sciences Corp., Lindon, UT). The 2% SELP solution with HRP and H₂O₂ was mixed and pipetted into the DSC sample chamber and allowed to gel at 4 °C before measurements. To capture the inverse transition temperature of SELP hydrogels, the 2% SELP hydrogels were equilibrated at the initial temperature for 10 min, and then heated in the sample chamber from 0 to 100 °C at a rate of 2 °C min⁻¹ and cooled to 0 °C at the same rate. The same volume of solvent was placed in the reference chamber during each scan. The baseline scans were taken with the solvent under the same condition and subtracted from the sample scans.

UV-Vis Spectrophotometry: The UV-vis spectra of SELP hydrogels were obtained by an Aviv 14DS UV-vis spectrophotometer equipped with a Peltier temperature controller (Aviv Biomedical, Lakewood, NJ). The 2% SELP solution with HRP and H₂O₂ was mixed and pipetted into a 1 mm path length absorption cuvette (Hellma USA, Plainview, NY) and allowed to gel at 4 °C before measurements. To capture the optical profiles of the 2% SELP hydrogels, wavelength scans were performed at 4 and 60 °C from 200 to 850 nm in 1 nm increments with an averaging time of 4 s per step. To characterize the inverse temperature transition of SELP hydrogel, temperature scans were performed at 350 nm from 0 to 60 °C at a rate of 2 °C min⁻¹ and then cooling to 0 °C at the same rate. Absorbance readings were taken after equilibrating SELP hydrogels at the desired temperature for 30 s. The averaging time of each measurement is 4 s per step. The baseline scans were taken with the solvent and cuvette under the same condition and subtracted from the sample scans.

Mechanical Tests: DMA studies were performed on a TA Instruments RSA3 dynamic mechanical analyzer (TA Instruments, New Castle, DE) with RSA-G2 immersion system. Cylindrical SELP hydrogels, ≈9 mm in diameter and 4 mm in thickness, were submerged in deionized water or buffers in the RSA-G2 solvent cup during DMA measurements. To assess the viscoelastic properties of the SELP hydrogels, the dynamic single point tests at a strain of 5%, with three different frequencies, 0.1, 1.0, and 10 Hz, were performed at 4, 10, 15, 22, 37, 50, and 60 °C with an equilibrium time of 30 min per step. The storage modulus, E', which is related to the elastic deformation, and the loss modulus, E'', which is related to the viscous deformation and energy absorption, were measured. To measure the Young's modulus of the SELP hydrogels, multiple extension mode tests were performed at a crosshead displacement rate of 0.01 mm s⁻¹ in compression direction. The Young's moduli were calculated by fitting the stress-strain curves in the linear response region of the SELP hydrogels (Figure S11, Supporting Information). Each sample type was run at least three times, and average values are reported.

Swelling and Deswelling Properties: The swelling ratio of the SELP hydrogels at 4 °C was determined by the ratio of the weight of the hydrogel equilibrated in deionized water to the weight of corresponding

as-prepared gel. For deswelling studies, the swollen samples equilibrated in deionized water at 4 °C were transferred to 4 °C buffer solution, and the deswelling ratio was determined by the ratio of the weight of the hydrogel in buffer to the weight of the hydrogel equilibrated in deionized water. To investigate the stimuli responsive properties, the hydrogels were equilibrated at 4, 10, 15, 22, 37, 50, and 60 °C in deionized water and buffers. The equilibrium deswelling ratio upon environmental stimulus is defined as the ratio of the weight of the hydrogel under the specific stimuli to the weight of the hydrogel equilibrated in deionized water at 4 °C.

Scanning Electron Microscopy: The microstructure of SELP hydrogels was imaged using a Zeiss Ultra55 SEM in the Center for Nanoscale Systems at Harvard University. SELP hydrogels were fast frozen by liquid nitrogen, freeze-dried, fractured to expose the cross-sections, and sputter coated with gold for SEM observation. Images were taken using SE2 detectors at 3.00 kV.

Cell Survival and Proliferation: hMSCs were isolated from fresh bone marrow aspirates (Lonza, Basel, Switzerland), cultured in Dulbecco's Modified Eagle Medium (supplemented with 10% fetal bovine serum, 0.1 × 10⁻³ M nonessential amino acids, 1 ng mL⁻¹ bFGF, 1% antibiotic/antimycotic), and seeded at passage 2, as previously described.^[4] For seeding, 2% SELP hydrogels of roughly 400 μm thickness were prepared as described above and allowed to cure overnight at 4 °C in fridge. Prior to seeding, hydrogels were extensively extracted with deionized water to remove residual reactants and then incubated in cell culture media for 4 h at 37 °C and 5% CO₂. Cells were seeded at a density of 200 cells per mm² allowed to adhere for 150 min prior to flooding with media. All cell culture was performed in an incubator maintained at 37 °C and 5% CO₂.

Cell Adherence and Viability: Cell adherence, confluence of growth, and viability were determined 14 d posterior to seeding, using LIVE/DEAD Viability/Cytotoxicity Kit (Life Technologies, Grand Island, NY) following the protocol recommended by the manufacturer. Briefly, cells were incubated with calcein AM and ethidium homodimer-1 (EthD-1) for 60 min to stain live (green) and dead cells (red), respectively. After staining the gels were washed three times with PBS and imaged using a fluorescence microscope (Keyence BZ-X700) with excitation at 488 nm and emission at 499–537 nm for live cells and excitation at 543 and emission at 620–650 nm for dead cells.

Replica Exchange Molecular Dynamics Simulations: Protein structure identification was performed with REMD simulations, using the CHARMM27 all-atom energy function.^[28] Replica exchange setup and analysis is carried out using Gromacs simulation software version 5.0.1.^[29] Visual molecular dynamics^[30] was used for visualization of protein structures. REMD enhances MD simulation by combining classical MD equilibration runs with the Monte Carlo method. This allows for wide conformational space sampling, avoiding protein entrapment in local-minima free energy states via thermal stimulation through high temperature replicas. Each REMD cycle includes an equilibration phase and an exchange event. Sixty replicas are used in simulation, with an initial input structure defined by an extended straight chain of amino acids. Temperatures for replicas are exponentially distributed between 280 and 400 K. The equilibration phase is 2 ps. Five thousand exchanges, based on the Metropolis criterion, are made per replica, for a total of 600 ns simulations for all replicas. Acceptance ratios for each molecule are between 30% and 45%, signifying sufficient sampling. Ensemble sampling is done for the last 8 ns for each temperature replica.

Supporting Information

Supporting Information is available from the Wiley Online Library or from the author.

Acknowledgements

The authors acknowledge the financial support of the NIH (U01 EB014976) and the Tissue Engineering Resource Center (NIH P41

EB002520) and the Air Force Office of Scientific Research. This work was performed in part at the Center for Nanoscale Systems (CNS), a member of the National Nanotechnology Infrastructure Network (NNIN), which is supported by the National Science Foundation under NSF award No. ECS-0335765. CNS is part of Harvard University.

Received: January 15, 2016

Revised: March 1, 2016

Published online: April 15, 2016

- [1] O. Wichterle, D. Lim, *Nature* **1960**, *185*, 117.
- [2] B. V. Slaughter, S. S. Khurshid, O. Z. Fisher, A. Khadernhosseini, N. A. Peppas, *Adv. Mater.* **2009**, *21*, 3307.
- [3] K. Y. Lee, D. J. Mooney, *Chem. Rev.* **2001**, *101*, 1869.
- [4] B. P. Partlow, C. W. Hanna, J. Rnjak-Kovacina, J. E. Moreau, M. B. Applegate, K. A. Burke, B. Marelli, A. N. Mitropoulos, F. G. Omenetto, D. L. Kaplan, *Adv. Funct. Mater.* **2014**, *24*, 4615.
- [5] H. G. Schild, *Prog. Polym. Sci.* **1992**, *17*, 163.
- [6] O. E. Philippova, D. Hourdet, R. Audebert, A. R. Khokhlov, *Macromolecules* **1997**, *30*, 8278.
- [7] a) C. M. Schilli, M. F. Zhang, E. Rizzardo, S. H. Thang, Y. K. Chong, K. Edwards, G. Karlsson, A. H. E. Muller, *Macromolecules* **2004**, *37*, 7861; b) L. L. Ren, T. X. Liu, J. A. Guo, S. Z. Guo, X. Y. Wang, W. Z. Wang, *Nanotechnology* **2010**, *21*, 335701; c) L. W. Xia, R. Xie, X. J. Ju, W. Wang, Q. M. Chen, L. Y. Chu, *Nat. Commun.* **2013**, *4*, 2226.
- [8] Y. Takashima, S. Hatanaka, M. Otsubo, M. Nakahata, T. Kakuta, A. Hashidzume, H. Yamaguchi, A. Harada, *Nat. Commun.* **2012**, *3*, 1270.
- [9] M. A. C. Stuart, W. T. S. Huck, J. Genzer, M. Müller, C. Ober, M. Stamm, G. B. Sukhorukov, I. Szleifer, V. V. Tsukruk, M. Urban, F. Winnik, S. Zauscher, I. Luzinov, S. Minko, *Nat. Mater.* **2010**, *9*, 101.
- [10] C. Geraths, E. H. Christen, W. Weber, *Macromol. Rapid Commun.* **2012**, *33*, 2103.
- [11] L. Dong, A. K. Agarwal, D. J. Beebe, H. R. Jiang, *Nature* **2006**, *442*, 551.
- [12] a) A. Sidorenko, T. Krupenkin, A. Taylor, P. Fratzl, J. Aizenberg, *Science* **2007**, *315*, 487; b) X. He, M. Aizenberg, O. Kuksenok, L. D. Zarzar, A. Shastri, A. C. Balazs, J. Aizenberg, *Nature* **2012**, *487*, 214.
- [13] a) J. D. Ehrick, S. K. Deo, T. W. Browning, L. G. Bachas, M. J. Madou, S. Daunert, *Nat. Mater.* **2005**, *4*, 298; b) N. Kong, Q. Peng, H. Li, *Adv. Funct. Mater.* **2014**, *24*, 4615; c) W. Yuan, J. Yang, P. Kopečková, J. Kopeček, *J. Am. Chem. Soc.* **2008**, *130*, 15760; d) W. Huang, A. Rollett, D. L. Kaplan, *Expert Opin. Drug Delivery* **2014**, *12*, 779.
- [14] a) D. W. Urry, T. L. Trapane, K. U. Prasad, *Biopolymers* **1985**, *24*, 2345; b) D. W. Urry, *J. Protein Chem.* **1988**, *7*, 1; c) D. W. Urry, *J. Protein Chem.* **1988**, *7*, 81.
- [15] D. W. Urry, C. H. Luan, T. M. Parker, D. C. Gowda, K. U. Prasad, M. C. Reid, A. Safavy, *J. Am. Chem. Soc.* **1991**, *113*, 4346.
- [16] D. W. Urry, S. Q. Peng, T. M. Parker, *Biopolymers* **1992**, *32*, 373.
- [17] a) D. E. Meyer, G. A. Kong, M. W. Dewhurst, M. R. Zalutsky, A. Chilkoti, *Cancer Res.* **2001**, *61*, 1548; b) J. R. McDaniel, I. Weitzhandler, S. Prevost, K. B. Vargo, M.-S. Appavou, D. A. Hammer, M. Gradzielski, A. Chilkoti, *Nano Lett.* **2014**, *14*, 6590; c) S. R. MacEwan, A. Chilkoti, *J. Controlled Release* **2014**, *190*, 314; d) X.-X. Xia, M. Wang, Y. Lin, Q. Xu, D. L. Kaplan, *Biomacromolecules* **2014**, *15*, 908; e) Y. Lin, X. Xia, M. Wang, Q. Wang, B. An, H. Tao, Q. Xu, F. Omenetto, D. L. Kaplan, *Langmuir* **2014**, *30*, 4406; f) Z. Megeed, M. Haider, D. Q. Li, B. W. O'Malley, J. Cappello, H. Ghandehari, *J. Controlled Release* **2004**, *94*, 433; g) R. Dandu, Z. Megeed, M. Haider, J. Cappello, H. Ghandehari, in *Polymeric Drug Delivery II: Polymeric Matrices and Drug Particle Engineering*, Vol. 924 (Ed: S. Svenson), American Chemical Society, Washington D.C., USA, 2006, p. 150.
- [18] X. X. Xia, Q. B. Xu, X. Hu, G. K. Qin, D. L. Kaplan, *Biomacromolecules* **2011**, *12*, 3844.
- [19] D. W. Lim, D. L. Nettles, L. A. Setton, A. Chilkoti, *Biomacromolecules* **2007**, *8*, 1463.
- [20] D. W. Urry, R. D. Harris, K. U. Prasad, *J. Am. Chem. Soc.* **1988**, *110*, 3303.
- [21] Q. Wang, X. Xia, W. Huang, Y. Lin, Q. Xu, D. L. Kaplan, *Adv. Funct. Mater.* **2014**, *24*, 4303.
- [22] S. Winkler, D. Wilson, D. L. Kaplan, *Biochemistry* **2000**, *39*, 12739.
- [23] J. N. Rodriguez-Lopez, D. J. Lowe, J. Hernandez-Ruiz, A. N. P. Hinerman, F. Garcia-Canovas, R. N. F. Thorneley, *J. Am. Chem. Soc.* **2001**, *123*, 11838.
- [24] W. Huang, S. Krishnaji, O. R. Tokareva, D. Kaplan, P. Cebe, *Macromolecules* **2014**, *47*, 8107.
- [25] A. Matsumoto, J. Chen, A. L. Collette, U. J. Kim, G. H. Altman, P. Cebe, D. L. Kaplan, *J. Phys. Chem. B* **2006**, *110*, 21630.
- [26] a) B. An, M. D. Tang-Schomer, W. W. Huang, J. Y. He, J. A. Jones, R. V. Lewis, D. L. Kaplan, *Biomaterials* **2015**, *48*, 137; b) X. Hu, M. D. Tang-Schomer, W. Huang, X.-X. Xia, A. S. Weiss, D. L. Kaplan, *Adv. Funct. Mater.* **2013**, *23*, 3875.
- [27] S. Sartori, V. Chiono, C. Tonda-Turo, C. Mattu, C. Gianluca, *J. Mater. Chem. B* **2014**, *2*, 5128.
- [28] T. Lazaridis, M. Karplus, *Proteins: Struct. Funct. Genet.* **1999**, *35*, 133.
- [29] M. Feig, J. Karanicolas, C. L. Brooks, *J. Mol. Graphics Modell.* **2004**, *22*, 377.
- [30] W. Humphrey, A. Dalke, K. Schulter, *J. Mol. Graphics Modell.* **1996**, *14*, 33.